JOURNAL OF Materials CHEMISTRY

# Synthesis and characterization of $SiO_2$–$Nb_2O_5$ systems prepared by the sol–gel method: structural stability studies

**Maria Suzana P. Francisco* and Yoshitaka Gushikem**

*Instituto de Química, Unicamp, CP 6154, 13083-970 , Campinas, SP, Brazil.*
*E-mail: suzana@iqm.unicamp.br*

***Received 18th January 2002, Accepted 17th April 2002***
***First published as an Advance Article on the web 22nd May 2002***

X-Ray diffraction (XRD), $N_2$ absorption (BET specific surface area), transmission electron microscopy (TEM), Raman and Fourier infrared (FT-IR) spectroscopic techniques have been applied to characterize the texture, structure and niobia–silica interaction of $SiO_2$–$Nb_2O_5$ systems prepared by the sol–gel method containing different amounts of $Nb_2O_5$ and calcined at temperatures between 393 and 1473 K. For a small loading of niobia, amorphous niobium species were well dispersed in the silica up to 1273 K. Crystallization is observed only after thermal treatment at 1473 K, with the T-phase predominating as observed by XRD and TEM analyses and confirmed by Raman spectra. For samples with a higher amount of niobia, the formation of a T-$Nb_2O_5$ phase was observed at 1273 K, and the H-$Nb_2O_5$ phase predominates at 1473 K. FT-IR results indicate the presence of Si–O–Nb linkages at the silica–niobia interface, formed during preparation, which are responsible for the higher structural stability of the $SiO_2$–$Nb_2O_5$ system. The stability of the $SiO_2$–$Nb_2O_5$ system is confirmed by obtaining high specific surface areas even after the high temperature of calcination.

## Introduction

The $SiO_2$–$Nb_2O_5$ system has been investigated for a large field of applications, such as methanol oxidation,[1,2] ethanol dehydrogenation,[3,4] partial methane oxidation,[5] selective adsorption and use as a biosensor after immobilizing mediator species.[6] The activity of this system is related to the coverage and the structural changes in the surface metal oxide overlayer.

In the same way that pure niobia possesses a quite complex crystalline morphologic behavior, the supported niobium oxide also exhibits polymorphism with thermal treatment. In general, pure $Nb_2O_5$ has an octahedrally coordinated $NbO_6$ structure in which distortions depend on how the polyhedrons are shared. Heating the $Nb_2O_5$ amorphous phase, the following crystallites, having different structures, are observed: TT and/or T phases (at *ca.* 773 K), B and/or M phases-$Nb_2O_5$ (at *ca.* 1073 K), and H phase (at *ca.* 1473 K).[7–9]

Taking into account that many factors can influence the crystallization behavior of pure and supported niobia,[7,10–12] it is very important to understand how the changes in the structure of $Nb_2O_5$ take place with experimental variables such as preparation method, nature of the oxide support, and thermal treatment.[4,7,13–15]

The stabilization of the active phase depends strongly on the characteristics of the support. The composition of a multicomponent oxide is a very important variable since it affects the formation of different niobium species, including superficial and crystalline bulk phases, and the reactivity also varies with the niobium oxide coverage.[14,16] Apart from its acid[16,17] and redox[1,18] properties, previous studies proved that the bridging Nb–O-support bonds formed in the $SiO_2$–$Nb_2O_5$ system are also responsible for decreasing the niobium species mobility.[11,13]

The optimization of a monolayer coverage of supported niobium oxide with different supports was studied and the following compositions were obtained for each case: $Al_2O_3$/ ~19 wt% $Nb_2O_5$, $TiO_2$/ ~7 wt% $Nb_2O_5$, $ZrO_2$/ ~5 wt% $Nb_2O_5$, and $SiO_2$/ ~2 wt% $Nb_2O_5$.[12] This difference in the coverage is assigned to the strength of the interaction of $Nb_2O_5$ and each specific substrate.[12,14,18,19]

The sol–gel processing method has proven to be a very suitable method, compared to conventional ones, such as impregnation, precipitation and grafting, to synthesize supported oxides with favorable textural properties, since it can improve active phase dispersion, allow for better control of sintering processes and stabilize the microstructure.[20–22]

In this work, our goal is to investigate the stability of the $SiO_2$–$Nb_2O_5$ system structure as a function of the niobium oxide loading and subsequent thermal treatment. The mixed oxides were prepared by the sol–gel method. To accomplish that goal, the $N_2$ physical absorption, X-ray diffraction (XRD), Raman and Fourier transform infrared (FT-IR) spectroscopies, and transmission electron microscopy (TEM) techniques were used.

## Experimental

The sol–gel method was employed to prepare $SiO_2$–$Nb_2O_5$ samples according to the following procedure. First, the TEOS (tetraethylorthosilicate) was pre-hydrolyzed and subsequently dissolved in ethanol in the molar proportion 1 : 3.8. Then, 0.86 ml of concentrated HCl solution was added to 50 ml of this solution. The resulting solution, called A, was refluxed at 353 K for 2.5 h. Another solution, called B, was prepared with $NbCl_5$ dissolved in 100 ml of ethanol (concentrations 0.22, 0.45, and 0.67 mol $l^{-1}$) under a $N_2$ atmosphere. The amounts of $NbCl_5$ were weighed in order to obtain Si and Nb final molar proportions of 1 : 0.05, 1 : 0.1 and 1 : 0.15. 50 ml of solution B was added to solution A; the mixture was stirred at room temperature for 3 h. After this time, 140 ml of $H_2O$ was slowly added to the mixture followed by stirring at room temperature for 2 h. Finally, the mixture was allowed to rest at 333 K until complete gelation. The solid was washed with water in a Buchner funnel several times and, after, with ethanol. Most of the solvent from the xerogel was evaporated at 383 K for 24 h, and the solid material was ground and sieved to 200 mesh. The final materials $SiO_2$–$Nb_2O_5$ (2.5, 5.0, and 7.5% in atomic units) were calcined in the temperature range of 423–1473 K.

The amounts of niobium determined by X-ray fluorescence were 5.0, 9.2, and 14.4% (in atomic units). The powdered samples thus prepared were designated as $SiO_2$–2.5% $Nb_2O_5$,

 DOI: 10.1039/b200685e

$SiO_2$–5.0% $Nb_2O_5$, and $SiO_2$–7.5% $Nb_2O_5$. Commercial amorphous $SiO_2$ (Fluka) was used in specific investigations.

The specific surface areas ($S_{BET}$) were measured by using the BET multipoint technique on a Micromeritics Flowsorb II 2300 connected to a flow controller. Prior to measuring, all the samples were degassed at 423 K for 16 h and finally outgassed to $10^{-4}$ Pa.

The X-ray powder diffraction patterns were obtained by using a Shimadzu XD-2A diffractometer with Cu-$K_\alpha$ radiation (40 kV/30 mA, $\lambda = 1.5405$ Å) and a graphite monochromator. The scanning range was 10–80° ($2\theta$) with a step size of 0.02° and a step time of 2.0 s. The identification of crystalline phases was accomplished by comparison with JCPDS file numbers 27-1312 and 32-0711, for $Nb_2O_5$ in the T and H phases, respectively.

The nano-sized crystallites of prepared powdered material were observed with HR-TEM (high-resolution transmission electron microscopy) on a JEOL JEM-3010 microscope operating at 300 keV. The powder was ultrasonically suspended in isopropyl alcohol and the suspension deposited on a copper grid previously covered with a thin layer of carbon ($\sim$30 Å).

The Raman spectra were recorded on a triple Jobin-Yvon T64000 Raman instrument equipped with a microscope and a CCD detection system. The spectra were obtained at room temperature using the 5145 Å line of an argon ion laser (Spectra Physics 2020 model) excited with an incident power of 1.65 mW for pure $SiO_2$ and $SiO_2$–$Nb_2O_5$ samples. The Raman scattering data were collected between 1200 and 150 $cm^{-1}$, with an integration time of 60 s and an accumulative number of 6.

The FTIR spectra in the range 4000–400 $cm^{-1}$ were recorded on a Bomen MB series FT-IR spectrophotometer. The FTIR technique was performed on 1 wt% samples diluted by previously dried KBr after the KBr/material had been pressed (KBr pellet technique). The FTIR-spectrum of a pellet of KBr was taken as a blank. The data were collected for $SiO_2$–$Nb_2O_5$/KBr pellets with 100 accumulative scans and 2 $cm^{-1}$ resolution.

## Results and discussion

### Specific surface area ($S_{BET}$)–$N_2$ adsorption

Fig. 1 shows the specific surface areas of $SiO_2$–2.5% $Nb_2O_5$, $SiO_2$–5.0% $Nb_2O_5$, and $SiO_2$–7.5% $Nb_2O_5$ samples after being calcined in the temperature range 423–1473 K.

According to the results, the BET areas of the samples depend on the amount of $Nb_2O_5$ dispersed in silica and on the thermal treatment. When the $SiO_2$–2.5% $Nb_2O_5$ sample is calcined at 423 K, the surface area is 940 $m^2\ g^{-1}$. Although the other two samples (5.0 and 7.5% of $Nb_2O_5$) treated at the same temperature also present high $S_{BET}$ (743 and 714 $m^2\ g^{-1}$, respectively), their $S_{BET}$ values correspond to a decrease of 23% (average value) with respect to the sample containing 2.5% niobium oxide. For all the compositions, the specific surface areas decrease with the temperature of calcination. Even after thermal treatment at 1073 K for 8 h, the sample with the lowest concentration of $Nb_2O_5$ shows the highest surface area (362 $m^2\ g^{-1}$). Independent of the temperature, the sample containing 7.5% niobium oxide presents the lowest surface area. At higher temperature (greater than 1273 K), all the samples present a drastic surface area reduction, with a value below the inferior detection limit of the equipment (8 $m^2\ g^{-1}$).

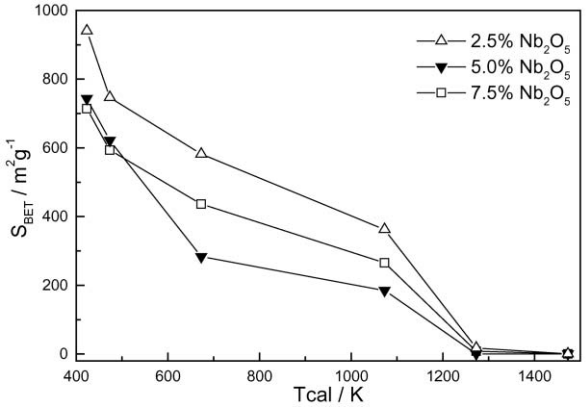


**Fig. 1** Specific surface areas of $SiO_2$–2.5% $Nb_2O_5$ (△), $SiO_2$–5.0% $Nb_2O_5$ (▼), and $SiO_2$–7.5% $Nb_2O_5$ (□) samples thermally treated in the range 423–1473 K.

Previously reported work showed that the surface area of $SiO_2$–$Nb_2O_5$ (2.7% $Nb_2O_5$ in atomic units) obtained by the grafting technique was stable under thermal treatment up to 773 K for 5 h, but its $S_{BET}$ value was only $\sim$310 $m^2\ g^{-1}$.[11] In this work by Denofre *et al.*, the interaction between superficial Si and Nb atoms explains the stabilization to higher treatment temperatures. Likely, the small surface area of the grafted material, compared to the $S_{BET}$ measured in the present work, is due to the pre-established textural features of the silica gel.

Besides the impregnation and co-precipitation methods, Morselli *et al.*[15] used sol–gel and functionalization of $SiO_2$ procedures to synthesize $SiO_2$–$Nb_2O_5$ systems with different molar ratios. Between the different methods, the sol–gel process starting from $Nb(OEt)_5$ in combination with $Si(OMe)_4$, $H_2C_2O_4(+NH_4F)$ as catalyst presented the highest $S_{BET}$ (628 $m^2\ g^{-1}$) for a silica–niobia system (molar ratio 50 : 1) thermally treated at 423 K. Making use of our sol–gel route with different starting materials, we obtained a niobia–silica material ($SiO_2$–7.5% $Nb_2O_5$ sample) treated at the same temperature with a slightly higher $S_{BET}$.

The textural characteristics of the aerogel niobia–silica system containing 2.5% of $Nb_2O_5$ thermally treated at 773 K for 2 h were studied[23] and the surface area measured is half the value measured for the $SiO_2$–7.5% $Nb_2O_5$ sample calcined at the same temperature.

The high surface areas are typical of silica and suggest that, even for a high-niobium oxide amount (7.5%), the silica framework is not so much affected by calcination at an intermediate temperature (1073 K). The decrease of the $S_{BET}$ of the samples thermally treated above 1273 K is a consequence of the sintering process.

Concerning the effect of the method of synthesis on the textural properties, the reaction pH is an important factor in determining the final properties of the material when processed by the sol–gel route. This method processed in highly acid condition results in uniform and small sized (between 0.5–3.0 nm) particles in both the sol and gel, so the final material has very high porosity.[21] In this sense, the HCl used as a catalyst is probably responsible for the very high specific surface area of the $SiO_2$–$Nb_2O_5$ samples obtained in this study.

### X-Ray diffraction analysis

Fig. 2 shows the diffractograms of the $SiO_2$–2.5% $Nb_2O_5$, $SiO_2$–5.0% $Nb_2O_5$, and $SiO_2$–7.5% $Nb_2O_5$ samples thermally treated at 423, 1073, 1273, and 1473 K, while Table 1 summarizes the corresponding crystallographic phases observed by XRD analyses. Neither the formation of a solid solution or the presence of some silica phase is observed.

Independent of the amount of niobium oxide, the diffractograms of the $SiO_2$–$Nb_2O_5$ samples calcined at low temperature ($\leqslant$1073 K, Fig. 2(a) and 2(b)), presented only a halo, no diffraction pattern is distinguishable. The lack of defined XRD peaks indicates that the niobium species are well dispersed on silica as crystallites smaller than 2–3 nm, which is the detection limit for Cu-K$\alpha$ radiation, or it is present as an amorphous phase.[13,23]

Otherwise, at higher temperatures of thermal treatment (1273 and 1473 K, Fig. 2(c) and 2(d), respectively), the XRD

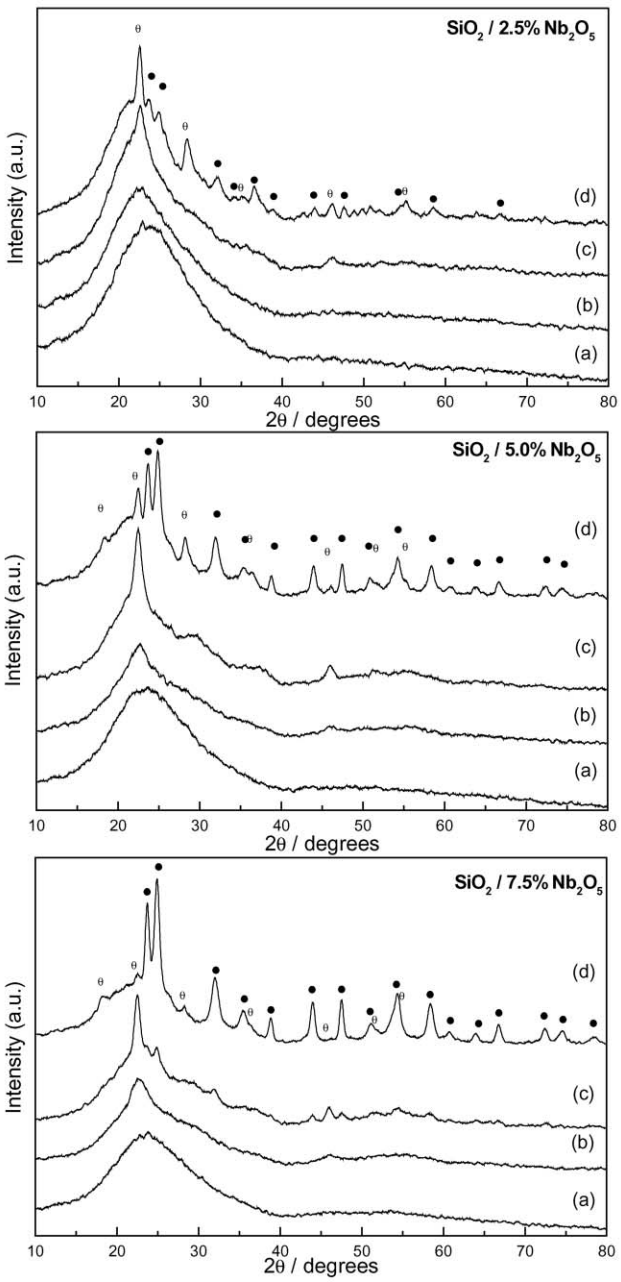


**Fig. 2** XRD patterns of $SiO_2$–2.5% $Nb_2O_5$, $SiO_2$–5.0% $Nb_2O_5$, and $SiO_2$–7.5% $Nb_2O_5$ samples thermally treated at 423 K (a), 1073 K (b), 1273 K (c), and 1473 K (d). $Nb_2O_5$ phases: T (θ) and H (●).

spectra show dependence on the niobium oxide content. The diffractogram of the $SiO_2$–2.5% $Nb_2O_5$ sample calcined at 1273 K shows only a wide halo (Fig. 2(c)). Despite the poor crystallization, the diffractogram of the $SiO_2$–5.0% $Nb_2O_5$ sample, also calcined at 1273 K, depicts two weak broad peaks centered at 22.4 and 46.0° (2θ), assigned to the T-$Nb_2O_5$ phase (JCPDS 27-1312, Fig. 2(c)). For the $SiO_2$–7.5% $Nb_2O_5$ sample thermally treated at the same temperature, the peaks related to the T-$Nb_2O_5$ phase become more pronounced and a second phase is also observed (JCPDS 32-0711), indicating a better reorganization of the amorphous solid containing higher amount of $Nb_2O_5$ (Fig. 2(c)). This second phase is attributed to H-$Nb_2O_5$ and the main peak is at 24.9° (2θ).

**Table 1** Crystallographic phases observed by XRD and Raman spectroscopy of $SiO_2$–$Nb_2O_5$ samples calcined at 1073, 1273, and 1473 K ($T_{cal}$)

| | Phases – XRD | | Phases – Raman | | |
|---|---|---|---|---|---|
| | $T_{cal}$ | | $T_{cal}$ | | |
| Samples | 1273 K | 1473 K | 1073 K | 1273 K | 1473 K |
| $SiO_2$–2.5%$Nb_2O_5$ | — | $T^H$, $H^L$ | — | $T^P$, H | $T^P$, H |
| $SiO_2$–5.0%$Nb_2O_5$ | $T^L$ | $T^M$, $H^H$ | T | $T^P$, H | T, $H^P$ |
| $SiO_2$–7.5%$Nb_2O_5$ | $T^M$ | $T^M$, $H^H$ | T | $T^P$, H | T, $H^P$ |

$^{L, M, H}$ low, medium and highly defined peaks. $^P$ the phase which predominates.

The H-$Nb_2O_5$ phase predominates for the samples containing 5.0 and 7.5% of niobium oxide calcined at 1473 K, even though the T-$Nb_2O_5$ phase is still quite observable (Fig. 2(d)). However, for the sample with less $Nb_2O_5$ (2.5%) calcined at 1473 K, the formation of the H-$Nb_2O_5$ crystallites is just beginning, as can be observed in Fig. 2(d).

There are studies in the literature reporting that silica stabilizes amorphous $Nb_2O_5$.[11,15] The relationship between structural stability and the interaction between two oxides was investigated.[17] When a strong interaction is established *via* Nb–O–Si linkages, the superficial $Nb_2O_5$ presents only the amorphous phase after thermal treatment at 773 K for 2 h. Even after 48 h of treatment at 1273 K, only weak peaks of diffraction were attributed to the TT-$Nb_2O_5$ phase.

A recent study on a monolayer of $Nb_2O_5$ deposited on $SiO_2$ reinforces the relation between crystallization and mobility.[13] The material was synthesized using two different routes in order to support $Nb_2O_5$, while the treatment temperature and its time were kept at 773 K and 12 h for both preparations. Using the precursor $NH^{4+}[Nb(C_2O_4)_3]^-$, the T and TT phases were present in the XRD spectrum. However, using the precursor $Nb(OC_2H_5)_5$, no diffraction patterns were observed due to a strong interaction between niobia and silica. Other synthetic routes have been taken to prepare $SiO_2$–$Nb_2O_5$ (molar ratio 20 : 1): sol–gel, precipitation/gelation and impregnation.[15] The XRD patterns of the system prepared by sol–gel (with different $Nb_2O_5$ starting precursors) revealed the appearance of a $Nb_2O_5$ crystallographic phase only at 1273 K, while diffraction peaks of $Nb_2O_5$ were seen in the material synthesized by precipitation/gelation and impregnation at 1173 and 873 K, respectively.

Our XRD results emphasize that the sol–gel process provided niobia supported in silica with specific characteristics: higher homogeneity, stability of microstructure, dispersion of active phase on the support, and specific surface area.[20,22,24,25] The sol–gel route adopted in this work, including experimental parameters and starting materials, stabilized the $Nb_2O_5$ amorphous phase up to 1273 K for the samples containing low amounts of niobia (2.5%) and up to 1073 K for the samples with higher amounts of $Nb_2O_5$ (5.0 and 7.5%).

Similar to our XRD results, diffraction peaks related to $Nb_2O_5$ crystallites have been identified for niobium oxide grafted on silica gel surfaces calcined at 1473 K (a system containing 2.7% of $Nb_2O_5$ in atomic units).[11] Nevertheless, these authors observed that at that temperature the silica was also crystallized. This fact was not observed for our XRD results. Maurer *et al.*[23] investigated the final structure of niobium oxide supported on silica aerogel *via* impregnation. The systems containing 0.05, 0.1, and 0.25 of monolayer fractions of niobia presented a dependence on the $Nb_2O_5$ amount. According to these authors, the sample with 0.05 coverage remained amorphous after thermal treatment at 1273 K for 2 h, indicating the presence of a stable highly dispersed superficial phase. In contrast, a TT-phase was observed for the higher coverage of niobia in this system (0.1 and 0.25 monolayer).

## HR-TEM micrographs

The TEM images of samples calcined up to 1073 K (not shown) present a homogeneous distribution of niobium oxide on the silica support. However, the micrographs reveal that the

samples treated at higher temperatures (1273–1473 K) are agglomerated as $Nb_2O_5$ crystallites on the silica mass (Fig. 3). Fig. 4 shows a TEM image at low magnification of a $SiO_2$–7.5% $Nb_2O_5$ sample calcined at 1473 K, which contains many nanocrystallites of encapsulated $Nb_2O_5$ (diameter $<25$ nm) on the amorphous silica texture.

Fig. 3 shows the micrographs of $SiO_2$–2.5% $Nb_2O_5$, $SiO_2$–5.0% $Nb_2O_5$, and $SiO_2$–7.5% $Nb_2O_5$ samples thermally treated at 1273 and 1473 K. The fringes appearing in the micrographs allow for identification of the crystallographic spacing of the $Nb_2O_5$ nanocrystallites. Depending on the amount of niobium oxide and the temperature of calcination, different fringes are observed and are related to T- and H-$Nb_2O_5$ nanocrystallites (see Table 2). The fringes most frequently observed correspond, respectively, to the 3.95 and 3.57 Å interplanar distances of T- and H-$Nb_2O_5$ phases.

In short, the same phases observed by XRD were identified by TEM images, which reinforces the observation that the behavior of the crystallization process occurs according to the

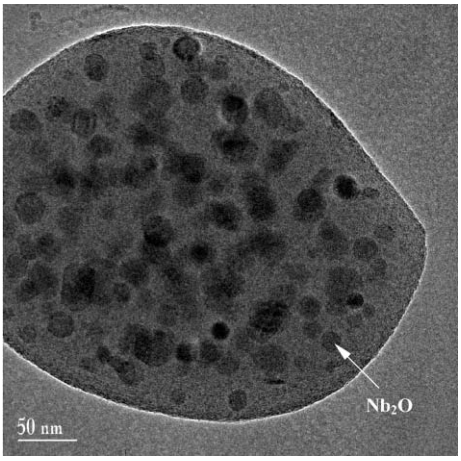


**Fig. 4** TEM micrograph in a low magnification of $SiO_2$–7.5% $Nb_2O_5$ sample thermally treated at 1473 K.

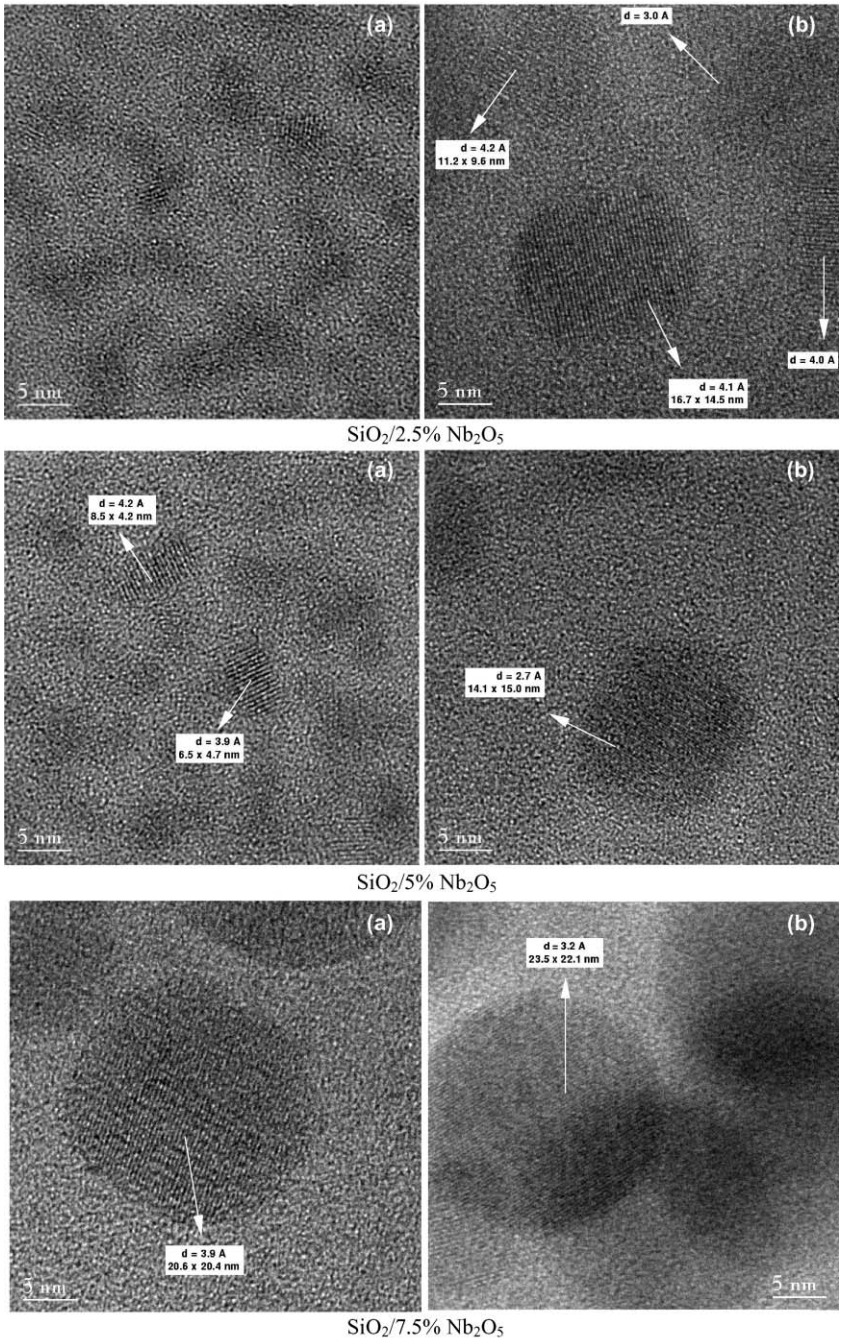


**Fig. 3** TEM micrographs of $SiO_2$–2.5% $Nb_2O_5$, $SiO_2$–5.0% $Nb_2O_5$, and $SiO_2$–7.5% $Nb_2O_5$ samples thermally treated at 1273 K (a) and 1473 K (b).

**Table 2** Crystallographic phases observed and niobia crystallite sizes obtained through TEM micrographs of $SiO_2$–$Nb_2O_5$ samples calcined at 1273 and 1473 K ($T_{cal}$)

| | Crystallite sizes of $Nb_2O_5$ ($\pm$10%/nm) – TEM | | | |
|---|---|---|---|---|
| | $T_{cal}$ | | $T_{cal}$ | |
| Samples | 1273 K T | 1473 K H | 1273 K T | 1473 K H |
| $SiO_2$–2.5%$Nb_2O_5$ | — | — | 14.7 | 6.8 |
| $SiO_2$–5.0%$Nb_2O_5$ | 6.1 | — | 19.8 | 16.8 |
| $SiO_2$–7.5%$Nb_2O_5$ | 7.8 | 7.0 | 19.6 | 21.1 |

concentration of niobia and to the thermal treatment. Moreover, the TEM images indicate an increase in $Nb_2O_5$ nanocrystallites with the amount of niobia and the thermal treatment (see Table 2).

### Raman spectroscopic data

The employment of Raman spectroscopy in the investigation of the molecular structures of the surface niobium oxide phases is interesting for two main reasons. First, silica does not exhibit Raman bands in the range 1000–100 $cm^{-1}$. So, even for the highest treatment temperature (1473 K), the only observable Raman bands are assigned to niobium oxide. Secondly, the T- and TT-$Nb_2O_5$ phases are easily confused in the XRD and TEM studies,[7,12] but the corresponding principal Raman bands are clearly distinguished (at 700 and 680 $cm^{-1}$, respectively, for pure $Nb_2O_5$ samples).

Table 1 summarizes the crystallographic phases observed by Raman spectroscopy of $SiO_2$–2.5% $Nb_2O_5$, $SiO_2$–5.0% $Nb_2O_5$, and $SiO_2$–7.5% $Nb_2O_5$ samples thermally treated at 1073, 1273 and 1473 K, the spectra are shown in Fig. 5.

For the sample containing the lowest amount of $Nb_2O_5$ ($SiO_2$–2.5%$Nb_2O_5$), no Raman features are observed for the sample calcined at 1073 K (Fig. 5(a)). The T-$Nb_2O_5$ phase predominates in the sample calcined at 1273 and 1473 K (bands at *ca.* 729 and 250 $cm^{-1}$)[18] while the H-$Nb_2O_5$ phase has its Raman bands (at *ca.* 989, 672, 627, 542, 307, and 258 $cm^{-1}$)[14,18–27] well defined only at 1473 K (Fig. 5(b) and 5(c)).

Otherwise, the Raman spectra of the samples with 5.0 and 7.5% of niobium oxide have a poorly defined band at *ca.* 720 $cm^{-1}$ attributed to the initialization of T-phase formation when they are thermally treated at 1073 K (Fig. 5(a)).[18] The intensities of the Raman bands assigned to the T-$Nb_2O_5$ phase increase after calcination at 1273 K, the Raman scattering of the H-$Nb_2O_5$ phase (small band at *ca.* 993 $cm^{-1}$) (Fig. 5(b)) is also observed. After the thermal treatment at 1473 K, both samples exhibit very defined Raman features of the H-$Nb_2O_5$ phase (bands at *ca.* 992, 899, 836, 673, 657, 629, 549, 468, 342, 303, 260, and 239 $cm^{-1}$)[14,18–27] (Fig. 5(c)).

As mentioned above, the Raman data are very useful to corroborate the XRD and TEM results that the crystallites of $Nb_2O_5$ of samples thermally treated above 1273 K are really T-phase. Furthermore, the fact that no Raman band is noted for a sample containing only 2.5% of $Nb_2O_5$ calcined above 1073 K confirms the species of niobium on silica are well dispersed in an amorphous phase.

### FT-IR analysis

The FT-IR spectra were obtained in order to compare the transmission bands of silica and $SiO_2$–$Nb_2O_5$ samples as a function of niobium oxide loading and thermal treatment. Fig. 6 shows the FT-IR of $SiO_2$–2.5% $Nb_2O_5$, $SiO_2$–5.0% $Nb_2O_5$, and $SiO_2$–7.5% $Nb_2O_5$ samples and pure silica calcined at 383, 1273 and 1473 K.

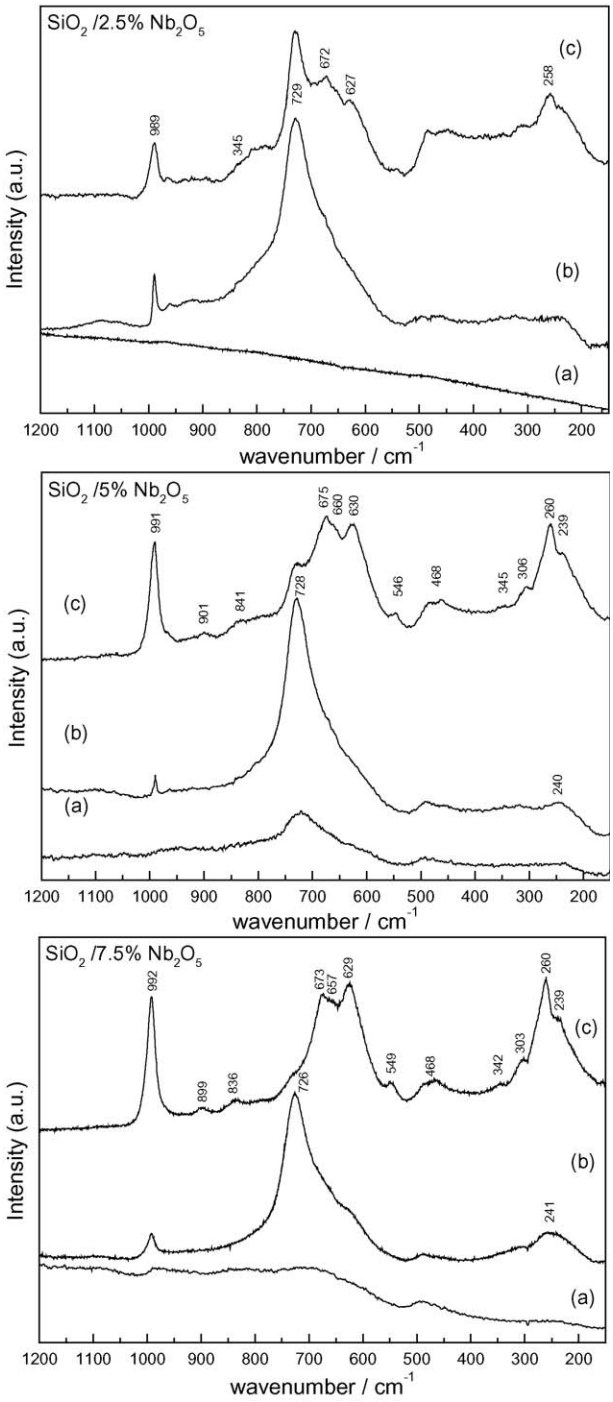


**Fig. 5** FT-Raman spectra of $SiO_2$–2.5% $Nb_2O_5$, $SiO_2$–5.0% $Nb_2O_5$, and $SiO_2$–7.5% $Nb_2O_5$ samples thermally treated at 1073 K (a), 1273 K (b), and 1473 K (c).

In the range 4000–2500 $cm^{-1}$, the spectra of all the samples exhibit a broad featureless band assigned to the stretching vibrations of $H_2O$ adsorbed on the silica surface (surface silanol groups, SiOH) perturbed by either intramolecular hydrogen bonding or with adsorbed water.[28–30] It was proved that the band at *ca.* 1636 $cm^{-1}$ is the result of overlap between the bending vibration mode of silanol groups and a weak overtone of bulk network modes.[30,31] Both bands seem to be less intense for the samples calcined at 1273 and 1473 K. Chun *et al.*[29] studied the $SiO_2$–$TiO_2$ system and the FT-IR bands at 3441 and 1635 $cm^{-1}$ decreased with an increase in the titanium oxide loading. For $SiO_2$–$Nb_2O_5$ samples, the different amounts of niobium oxide do not change the intensity of the same bands.

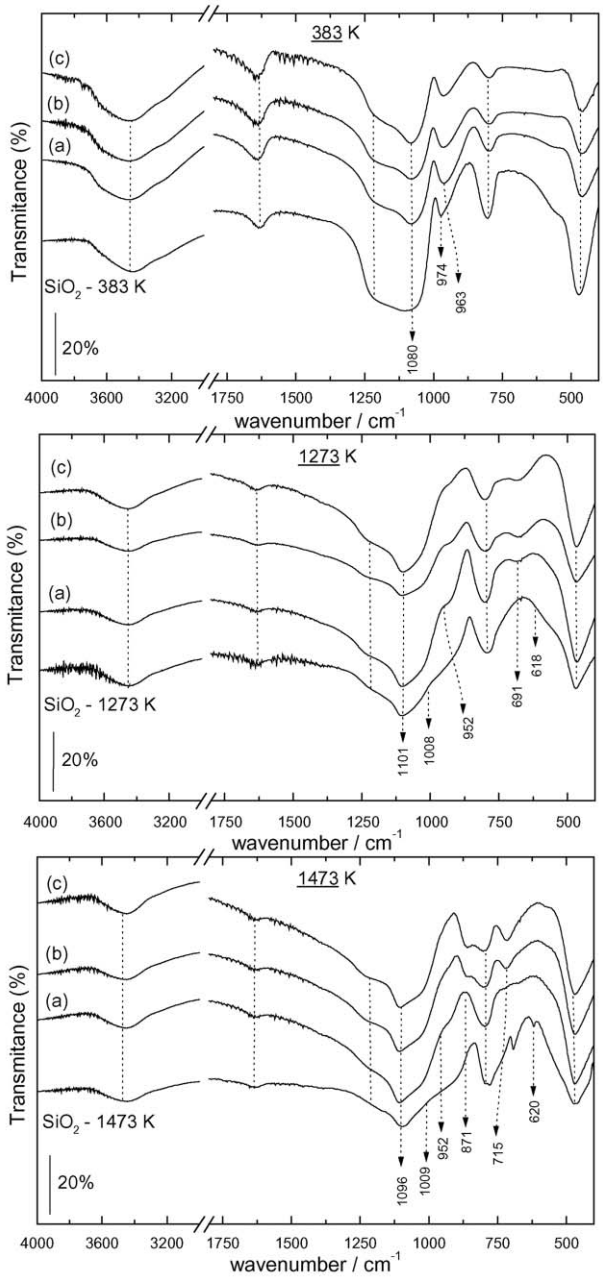


**Fig. 6** Transmission FT-IR spectra of $SiO_2$–2.5% $Nb_2O_5$ (a), $SiO_2$–5.0% $Nb_2O_5$ (b), and $SiO_2$–7.5% $Nb_2O_5$ (c) samples thermally treated at 1073 K, 1273 K, and 1473 K.

The FT-IR spectrum of silica treated at 383 K (dried gel) shows the characteristic bands (at 1218, 1080, 804 and 461 $cm^{-1}$) of fused quartz.[32] The band at wave number near 1218 $cm^{-1}$ corresponds to the longitudinal optic mode (LO) of the asymmetric stretching vibration of Si–O–Si bond and that at 1080 $cm^{-1}$ to the transversal optic mode (TO).[29,30,33] The band at 804 $cm^{-1}$ has been assigned to the symmetric stretching vibration mode of Si–O–Si bond in the bulk network, and that near 461 $cm^{-1}$ to the out-of-plane bending vibration mode of Si–O–Si bond in the network structure.[30,32] These four bands, for all the silica–niobia samples dried at 383 K, are similar but, compared to the bands of pure silica, these bands have a lower intensity.

The featureless bands of the fused quartz observed in the FT-IR spectra of the samples and of silica treated at 1273 K are slightly intensified, when compared to the spectra of the material dried at 383 K, except for the band at 1080 $cm^{-1}$. This result reinforces the stability of the amorphous silica, also discussed in the other analysis. Otherwise, the band at 1080 $cm^{-1}$ appears shifted to higher wave number values, *ca.* 1101 $cm^{-1}$, for samples treated at higher temperature (1273–1473 K). According to the literature,[28,33] this band is attributed to the asymmetric stretching vibration of the Si–O–Si bond and the shifting to higher wave number values is due to the higher density of the material structure. Therefore, the FT-IR spectra of samples thermally treated at the different temperatures present a progressive structural transformation from gel (at 383 K) to a better-organized structure of fused quartz after being treated at 1273 K.

In general for the mixed oxides, the FT-IR band at *ca.* 960 $cm^{-1}$ has been frequently discussed in the literature, but there are still controversies concerning this band. For the $SiO_2$–$TiO_2$ system, some authors assume that the band between 970–950 $cm^{-1}$ is due to the stretching of silanol groups.[29,30,34] The intensity is believed to increase with respect to the intensity of the bending vibration mode of Si–O–Si band with an increase of titanium loading and disappears after higher treatment temperatures.[34] According to Chun *et al.*,[29] the band due to Ti–O–Si vibration is weak, being covered by the peak at 970 $cm^{-1}$ for the silanol groups.

In a different way, the structure of *mesoporous* crystalline iron-modified MCM-41 materials was investigated by FT-IR and the band at 960 $cm^{-1}$ was assigned to Si–O–Fe vibrations.[35] The FT-IR technique was also employed in the study of the structure of manganese-modified MCM-41 materials. The authors stated that Mn ions have been incorporated into the framework of the Si–O bond, giving origin to a Si–O–Mn vibration near 968 $cm^{-1}$.[32] A recent study concerning the effects of the addition of poly(ethylene glycol) on the formation of anatase nanocrystallites in $SiO_2$–$TiO_2$ films observed a band *ca.* 950 $cm^{-1}$ which was also assigned to the Si–O–Ti bond.[36]

In the present work, the spectrum of dried silica at 383 K shows an absorption band at *ca.* 976 $cm^{-1}$ due to the stretching of silanol groups, SiOH. This band is less intense for silica calcined above 1473 K, in agreement with other authors.[34] The spectra of the samples with niobia added present this band shifted to lower wave numbers (952 $cm^{-1}$), being more pronounced for the $SiO_2$–2.5% $Nb_2O_5$ sample heat treated at 1273 K. This result probably shows a Si–O–Nb bond at the silica–niobia interface. The decrease of its intensity with the calcination temperature can be explained by the fact that, under these conditions, agglomeration of niobia takes place, as also observed by XRD, TEM and Raman spectroscopy analyses.

Therefore, the surface interactions between niobia and silica are responsible for niobia stabilization, avoiding crystallization. Probably, the established interactions prevent niobia mobility. It is known that how $Nb_2O_5$ crystallization takes place can be different according to the interactions between the components. Considering this fact, the structure of pure $Nb_2O_5$ is very different when it is in a system with multi-components. The interactions between $Nb_2O_5$ and another species affect its mobility and, consequently, the final structure. Both the nature of the support and the method of synthesis have a great influence on the formation of superficial species present in the mixed oxides.

The $SiO_2$–$Nb_2O_5$ system has been studied previously[15] and the authors concluded that a strong interaction between niobium and silica oxides is established during the sol–gel process, *i.e.*, it involves the formation of Si–O–Nb bonds. This conclusion was arrived at by the observation of a FT-IR band between 930–920 $cm^{-1}$ that disappears with the agglomeration process, after treatment at high temperature.

The FT-IR spectra of $SiO_2$–5.0% $Nb_2O_5$ and $SiO_2$–7.5% $Nb_2O_5$ samples calcined at 1473 K present two weak supplementary bands, at 871 and 715 $cm^{-1}$. This fact could be related to the number of phases found in XRD analyses and, consequently, indicates a more heterogeneous structure after the thermal treatment. Furthermore, it shows that the sample

containing 2.5% of $Nb_2O_5$ supported on silica has a better dispersion than the samples with higher amounts of niobia, in agreement with the other techniques.

According to Denofre *et al.*,[11] the band at *ca.* 620 $cm^{-1}$ is due to the vibration of the polysiloxane rings in niobia grafted on a silica surface. They observed that the band appears only after the thermal treatment at 1473 K and, above this temperature, the formation of these rings is not observed, indicating the stability of the structure. The same band was observed in the FT-IR spectra of the $SiO_2$–$TiO_2$ system prepared by the sol–gel method.[33] The authors confirmed the pronounced growth of the trisiloxane rings above 1373 K. Pure $SiO_2$ and $SiO_2$–$Nb_2O_5$ obtained by the grafting process thermally treated at 1273 and 1573 K, respectively, showed the FT-IR band at 622 $cm^{-1}$, which was assigned to an α-cristobalite phase and, as indicated by XRD, in a smaller amount than the quartz phase.[37]

The FT-IR spectra of silica calcined at 1473 K presents a very pronounced band at *ca.* 622 $cm^{-1}$. Since the XRD pattern of pure silica is observable only after thermal treatment at 1473 K (not shown) and the only phase is fused quartz, the FT-IR band is probably associated with the formation of polysiloxane rings. The fact that this band is not identified in our $SiO_2$–$Nb_2O_5$ samples shows the good thermal stability of silica in the presence of niobia.

## Conclusions

The sol–gel synthesis method provides the $SiO_2$–$Nb_2O_5$ system with stability since, even after a high treatment temperature (1073 K), the samples maintain a high surface area and their structures remain completely amorphous. The Nb–O–Si linkages on the surface, formed during the preparation, give rise to the higher structural stability of the $SiO_2$–$Nb_2O_5$ system, since both the support nature and the method of synthesis have a great influence on the formation of superficial species present in mixed oxides. The loading of niobium oxide is important because it affects species formation under thermal treatment. The sample with the lowest amount of metal oxide, *i.e.*, $SiO_2$–2.5% $Nb_2O_5$, has niobia nanocrystallites in an amorphous phase on silica until a treatment temperature as high as 1073 K.

## Acknowledgement

The research work was partially performed at the *Grupo de Propriedades Ópticas* (GPO) of the IFGW-UNICAMP, and *Laboratório de Microscopia Eletrônica* (LME) of the National Synchrotron Light Laboratory (LNLS), Brazil. The authors wish to acknowledge Prof. Carol H. Collins (IQ-UNICAMP) for manuscript revision. M.S.P. Francisco is indebted to the São Paulo State Research Funding Institution, FAPESP (grant 01/01248-9) for a Postdoctoral fellowship.

## References

1 X. Gao, I. E. Wachs, M. S. Wong and J. Y. Ying, *J. Catal.*, 2001, **203**, 18.
2 I. E. Wachs, J.-M. Jehng, G. Deo, H. Hu and N. Arora, *Catal. Today*, 1996, **28**, 199.
3 A. Yamaguchi, K. Asakura and Y. Iwasawa, *J. Mol. Catal. A*, 1999, **146**, 65.
4 N. Ichikuni, M. Shirai and Y. Iwasawa, *Catal. Today*, 1996, **28**, 49.
5 F. Arena, F. Frusteri, A. Parmaliana and N. Giordano, *J. Catal.*, 1993, **143**, 299.
6 C. A. Pessoa and Y. Gushikem, *J. Electroanal. Chem.*, 1999, **184**, 236.
7 E. I. Ko and J. G. Weissman, *Catal. Today*, 1990, **8**, 27.
8 I. Nowak and M. Ziolek, *Chem. Rev.*, 1999, **99**, 3603.
9 A. A. McConnel, J. S. Anderson and N. R. Rao, *Spectrochim. Acta, Part A*, 1975, **32**, 1067.
10 I. E. Wachs, L. E. Briand, J.-M. Jehg, L. Burcham and X. Gao, *Catal. Today*, 2000, **57**, 323.
11 S. Denofre, Y. Gushikem, S. C. Castro and Y. Kawano, *J. Chem. Soc., Faraday Trans.*, 1993, **89**, 1057.
12 J.-M. Jehng and I. E. Wachs, *J. Mol. Catal.*, 1991, **67**, 369.
13 E. B. Pereira, M. M. Pereira, Y. L. Lam, C. A. C. Perez and M. Schmal, *Appl. Catal. A*, 2000, **197**, 99.
14 J.-M. Jehng and I. E. Wachs, *Catal. Today*, 1993, **16**, 417.
15 S. Morselli, P. Moggi, D. Cauzzi and G. Predieri, *Stud. Surf. Sci. Cat.*, 1998, **118**, 763.
16 J. Datka, A. M. Turek, J. M. Jehng and I. E. Wachs, *J. Catal.*, 1992, **135**, 186.
17 P. A. Burke, J. G. Weissman, E. I. Ko and P. Wynblatt, in *Catalysis*, ed. J. W. Wards, Elsevier, Amsterdam, 1987, p. 457.
18 J.-M. Jehng and I. E. Wachs, *Catal. Today*, 1990, **8**, 37.
19 L. J. Burcham, J. Datka and I. E. Wachs, *J. Phys. Chem.*, 1999, **103**, 6015.
20 A. Martínez-Arias, M. Fernández-García, J. Soria and J. C. Conesa, *J. Catal.*, 1999, **182**, 367.
21 R. D. Gonzalez, T. Lopez and R. Gomez, *Catal. Today*, 1997, **35**, 293.
22 C. J. Brinker and G. W. Scherer, *Sol-Gel Science: the Physics and Chemistry of Sol-Gel Processing*, Academic Press Limited, 1993.
23 S. M. Maurer, D. NG and E. I. Ko, *Catal. Today*, 1993, **16**, 319.
24 R. K. Iler, *The Chemistry of Silica*, Wiley, New York, 1979.
25 L. L. Murrell, *Catal. Today*, 1997, **35**, 225.
26 I. Wachs, *Catal. Today*, 1996, **27**, 437.
27 U. Balachandran and N. G. Eror, *J. Mater. Sci. Lett.*, 1982, **1**, 374.
28 E. Péré, H. Cardy, O. Cairon, M. Simon and S. Lacombe, *Vib. Spectrosc.*, 2001, **25**, 163.
29 H. Chun, Y. Wang and T. Hongxiao, *Appl. Catal. B*, 2001, **30**, 277.
30 K. Ogura, K. Nakaoka, M. Nakayama, M. Kobayashi and A. Fuji, *Anal. Chim. Acta*, 1999, **384**, 219.
31 K. M. Davis and M. Tomozawa, *J. Non-Cryst. Solids*, 1995, **185**, 203.
32 S. W. Wang, X. X. Huang, X. X. , J. K. Guo, J. K. and B. S. Li, *Mater. Lett.*, 1996, **28**, 43.
33 C. C. Perry, X. Li and D. N. Waters, *Spectrochim. Acta*, 1991, **47**, 1487.
34 M. R. Boccuti, K. M. Rao; A. Zecchina, G. Leofanti and G. Petrini, in *Structure and Reactivity in Surfactants*, ed. G. Morterra and A. Zecchina, Elsevier, Amsterdam, 1989, p.133.
35 Z. Y. Yuan, S. Q. Liu, T. H. Chen, J. Z. Wahng and H. X. Li, *J. Chem. Soc., Chem. Commun.*, 1995, 973.
36 Y. Kotani, A. Matsuda, T. Kogure, M. Tatsumisago and T. Minami, *Chem. Mater.*, 2001, **13**, 2144.
37 Y. Kawano, S. Denofre and Y. Gushikem, *Vib. Spectrosc.*, 1994, **7**, 293.